

Augmented Reality for Robots (ARRO): Pointing Visuomotor Policies Towards Visual Robustness

Reihaneh Mirjalili^{*1}, Tobias Jülg^{*1}, Florian Walter¹, Wolfram Burgard¹

^{*}Equal contribution

¹Department of Computer Science & Artificial Intelligence, University of Technology Nuremberg

Abstract: Visuomotor policies trained on human expert demonstrations have recently shown strong performance across a wide range of robotic manipulation tasks. However, these policies remain highly sensitive to domain shifts stemming from background or robot embodiment changes, which limits their generalization capabilities. In this paper, we present ARRO, a novel calibration-free visual representation that leverages zero-shot open-vocabulary segmentation and object detection models to efficiently mask out task-irrelevant regions of the scene without requiring additional training. By filtering visual distractors and overlaying virtual guides during both training and inference, ARRO improves robustness to scene variations and reduces the need for additional data collection. We extensively evaluate ARRO with Diffusion Policy on several tabletop manipulation tasks in both simulation and real-world environments, and further demonstrate its compatibility and effectiveness with generalist robot policies, such as Octo and OpenVLA. Across all settings in our evaluation, ARRO yields consistent performance gains, allows for selective masking to choose between different objects, and shows robustness even to challenging segmentation conditions. Videos showcasing our results are available at: augmented-reality-for-robots.github.io

Keywords: Domain Adaptation, Imitation Learning, Scene Abstraction

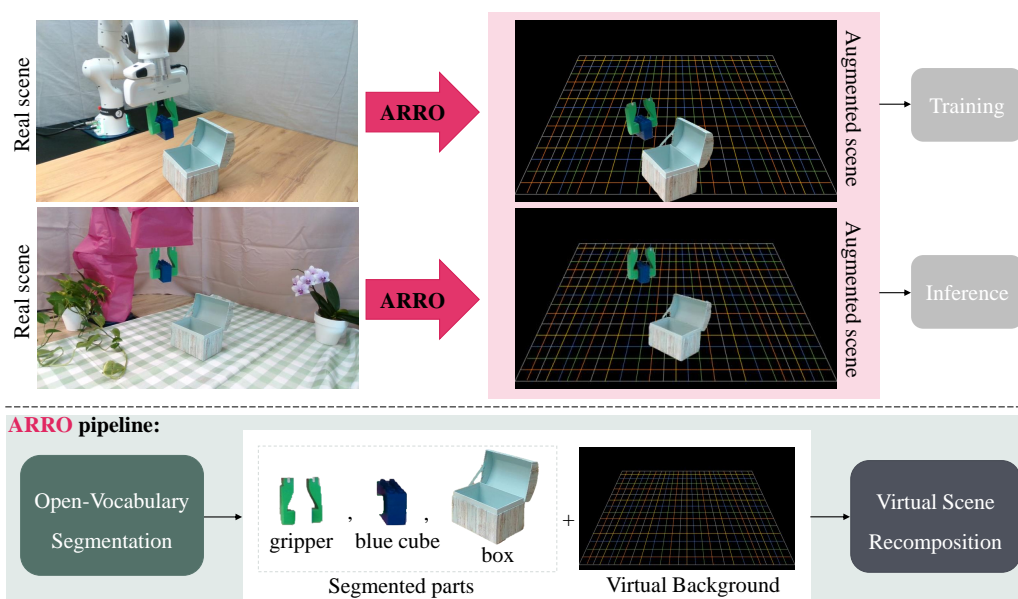


Figure 1: **ARRO in a nutshell:** Our pipeline segments the robot gripper and task-related using open-vocabulary vision models and overlays them onto a virtual background. We consistently use this process across training and inference to enhance robustness against visual domain shifts.

1 Introduction

Visuomotor policy learning in robotics has recently benefited significantly from advances in generative modeling [1, 2, 3]. State-of-the-art methods for imitation learning from human expert demonstrations show strong performance in both tabletop and mobile manipulation tasks [4, 5, 6], which has motivated the collection of a vast range of robotics datasets [7, 8, 9, 10, 11] and concerted efforts to curate and share them [12]. This has enabled the development and training of large-scale visuomotor policies that are commonly referred to as robotics foundation models and cover a wide range of tasks, robots, and environments [12, 13, 14, 15, 16].

Ideally, visuomotor policies should be robust to visual environment changes and agnostic to the robot’s appearance. However, despite the generalization capabilities that some of these policies achieve in specific scenarios, generalization under domain shift remains a challenge. Even subtle visual changes—such as background variation, distractor objects, or differences in the appearance of the robot—that occur when a policy is deployed in conditions different from those seen during training can lead to notable performance degradation [17, 18]. This severely limits the applicability of such policies in real-world environments, where visual variability is inevitable. Although increasing the diversity of the training data can partially mitigate these issues, such strategies are costly and often fail to cover the full spectrum of real-world variation.

To address these challenges, we propose a shift in perspective motivated by recent developments in foundation models for computer vision. Instead of training policies to handle every possible visual scenario, we aim to transform the input space to a canonical representation that cancels out scene variations not relevant for the task. Concretely, we ask: *Can we equip robots with a task-oriented augmented reality view that selectively filters irrelevant information and emphasizes only what is essential for task execution?*

In this paper, we introduce **ARRO** (Augmented Reality for **RO**bots), a method that functions like *AR glasses* for robots—minimizing visual distractions, highlighting task-relevant elements, and enhancing policy robustness without requiring retraining. ARRO is a calibration-free visual pre-processing pipeline for generating task-specific augmented visual observations. By leveraging open-vocabulary segmentation and object detection, it retains only the robot gripper and the target objects, and overlays them onto a structured virtual background. This process results in a consistent, simplified input space that supports visuomotor robustness across varied environments and embodiments.

In summary, we make the following contributions: (1) We propose ARRO, a calibration-free augmented reality pipeline that improves the robustness of visuomotor policies by selectively retaining task-relevant visual information—specifically, the robot gripper and manipulated objects—while masking out distractors. (2) We introduce ARRO’s system design, which is based on vision-language models and computer vision foundation models for segmentation and object detection. As a result, it operates in an open-vocabulary and zero-shot manner. Neither camera calibration nor training is required. In principle, ARRO can be combined with any visuomotor policy. (3) We create a virtual background with clear visual references that is included in the virtual scene. Our experimental results show that this improves performance compared to a uniform background without visual markers. (4) We evaluate ARRO in multiple tasks and settings on Diffusion Policy [4], Octo [15], and OpenVLA [16]. Our results show substantial improvements in robustness against changes in background and embodiment and the presence of distractors.

2 Related Works

Domain Adaptation in Imitation Learning Domain adaptation has been a long-standing research topic in robotics, particularly for visuomotor policies. In the context of reinforcement learning, it is especially relevant when transferring a policy trained in simulation to the real world and can be addressed, for example, through domain randomization [19, 20]. In imitation learning, large-scale datasets have emerged as a key strategy for enabling generalization in robot learning across varied tasks, embodiments, and environments. The Open X-Embodiment dataset [12] consolidates

demonstrations from a wide range of robotic platforms and has enabled the training of generalist robot policies [12, 15, 16]. Given the cost of collecting large-scale robot data, several works leverage human videos [21, 22, 23]. Another line of work addresses embodiment differences by using wrist-mounted cameras [24, 25], which maintain consistent robot-centric viewpoints but cannot leverage the large amount of available third-person data and are limited in tasks requiring broader scene understanding. In contrast, ARRO operates directly on third-person data without retraining or new data collection.

Environment Representations for Visuomotor Manipulation Policies Presentations of the environment that are robust against domain shift are a long-standing research topic in robot learning. Object-centric representations [26, 5] aim to extract task-relevant objects from the scene while excluding everything else. In contrast, ARRO performs the same operation directly in image space and does not require any training. Transporter networks [27] extend the idea of object-centric representation by not only identifying relevant objects but also outputting corresponding actions that can be conditioned on language [28]. Another line of work leverages keypoints and constraints between them to represent objects and goal poses of manipulation tasks [29, 30]. Recently, foundation models were used to generate both keypoints and constraints automatically [31]. Vision-language models have also been shown to operate entirely without keypoints by reasoning over visual annotations in the camera image [32, 33]. A disadvantage of keypoint-based methods is that they make implicit assumptions about the types of tasks to be executed. More general approaches learn representations from large datasets, such as human videos [34, 35] and also support 3D data [36].

Visual Editing Most closely related to our approach are methods that apply direct visual editing to RGB camera images. Several works augment training data by synthesizing new backgrounds, tasks, or distractor objects [37, 38, 39, 40, 41]. Other approaches focus on adapting visual inputs for cross-embodiment transfer and scene variations. Zhang et al. [42] apply style transfer methods to transform real-world camera images to synthetic images that capture the style of the simulation environment which was used for training. Mirage [43] enables zero-shot cross-embodiment transfer via cross-painting—masking the target robot, inpainting missing regions, and overlaying rendered source robot images. While effective for robot arm transfer, it requires precise camera calibration, URDF files, and does not handle background shifts. Lepert et al. [44] overlay robot segmentation masks for embodiment transfer without new data collection, but still require policy retraining, static backgrounds, and precise calibration. RoVi-Aug [45] augments robot datasets using fine-tuned diffusion models to generate new robot embodiments and camera viewpoints. However, it requires paired data, additional training, and does not address background variation. In contrast, our method filters out irrelevant visual information via open-vocabulary segmentation, achieving robustness to background and embodiment changes without needing calibration, retraining, or extra data.

3 Approach

Problem Formulation We adopt the standard visuomotor control setting, where at each time step t , a robot observes a camera frame I_t and executes an action a_t based on a policy $\pi(a_t, \dots, a_{t+T_a} \mid I_{t-T_o}, \dots, I_t)$ with observation horizon T_o and action horizon T_a . Throughout this paper, I_t is an RGB camera image and a_t an absolute or relative task space action. π is trained on a source-domain dataset of expert demonstrations $\mathcal{D}_{\text{train}} = \{(I_t, a_t)\}$. When deployed in a target domain $\mathcal{D}_{\text{test}}$ with novel backgrounds, distractor objects, or changes in robot embodiment, such policies often fail due to sensitivity to irrelevant visual variations. Our objective is to compute a calibration-free visual transform $\Phi(I_t) = \tilde{I}_t$ that takes as input the unaltered image I_t and outputs the corresponding augmented image \tilde{I}_t which only contains task-relevant elements. We design Φ based on state-of-the-art vision models to enable zero-shot open-vocabulary object detection without training and apply a calibration-free initialization scheme that leverages a vision-language model. ARRO can thus be deployed without any setup-specific adjustments.

Open-Vocabulary Segmentation To isolate the robot gripper and task-related objects, we employ a two-phase segmentation process, consisting of an initial segmentation on the first incoming frame, followed by temporally consistent segmentation propagation over time. At the start of an episode, we apply an open-vocabulary object detection model (e.g., Grounding DINO [46]), prompted with the object class label c , to the first frame I_0 , yielding a bounding box:

$$B_0 = \text{Detect}(I_0, c) \quad (1)$$

This bounding box can then be used to extract the object with a promptable segmentation model like SAM 2 [47]. Segmenting the gripper requires a different approach. Standard object detection models are not well-suited for detecting robot grippers, as such objects are typically underrepresented in the training data. Therefore, to segment the gripper, we first apply standalone segmentation same frame, producing a set of region proposals without any prompts:

$$\{S_0^i\}_{i=1}^N = \text{Segment}(I_0) \quad (2)$$

The original image is then annotated by placing numbered labels at the center of each segmented region. This annotated image, denoted as I_0^* , is passed to a vision-language model (e.g., GPT-4o [48]) to identify the regions corresponding to the gripper fingers:

$$g_0 = \text{VLM}(I_0^*) \quad (3)$$

The output $g_0 = \{(x_\ell, y_\ell), (x_r, y_r)\}$ represents the detected keypoints for the left and right gripper fingers, respectively. This approach also works for objects that have a simple shape and therefore can be segmented without a bounding box. Next, using the object bounding box B_0 and the gripper keypoints g_0 as prompts, we apply a memory-based segmentation model to extract segmented regions:

$$S_0^{\text{obj}}, S_0^{\text{grripper}} = \text{Segment}(I_0 \mid B_0, g_0) \quad (4)$$

In our experiments, we are using SAM 2 [47]. Once the initial segmented parts are obtained, we track the gripper and object regions, S_t^{grripper} and S_t^{obj} , across all subsequent frames I_t for $t > 0$, by conditioning on the memory accumulated during earlier frames [47]. This enables temporally consistent segmentation over time without requiring re-identification or additional supervision.

Virtual Scene Recomposition Once the relevant segmentations are obtained at each timestep t , we extract the task-relevant regions by computing the union $S_t = S_t^{\text{obj}} \cup S_t^{\text{grripper}}$, where S_t^{obj} and S_t^{grripper} denote the binary masks for the object and the robot gripper, respectively. We then overlay S_t on a simple black background or a hand-crafted colored grid that is reused across all sequences. While not photorealistic, this background provides visual cues and consistency across frames. The final background-augmented image, \tilde{I}_t , is computed as:

$$\tilde{I}_t = S_t \odot I_t + (1 - S_t) \odot B, \quad (5)$$

where B is the selected background image, and \odot denotes element-wise multiplication. This augmentation process is applied to all frames in $\mathcal{D}_{\text{train}}$ and runs in real time during inference.

4 Experimental Results

4.1 Real-World Experiments

We conduct four real-world tabletop manipulation tasks using a Franka Research 3 (FR3) robot arm with custom 3D-printed fingers, as illustrated in Figure 2. The tasks include: (a) picking up a single cube, (b) pushing the cube to a red cross location, (c) placing a plush octopus next to a doll, and (d) dropping a cube into a box and closing the lid. These tasks were selected to evaluate a range of manipulation behaviors under realistic visual conditions. For each task, we collect 90 human demonstrations to support learning and evaluation.

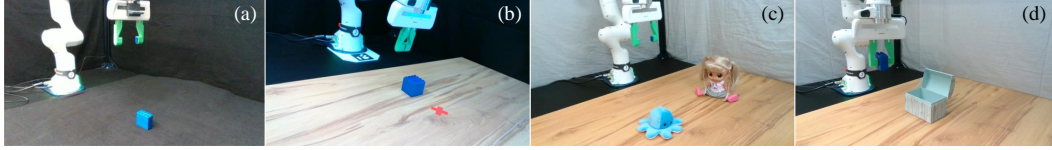


Figure 2: Experiment setups for our (a) pick-v1, (b) push-v1, (c) doll-v1 and (d) box-v1 tasks.

4.1.1 Performance Across Domain Shifts

In this section, we evaluate whether ARRO mitigates the degradation in policy performance caused by visual domain shifts. To assess robustness, we introduce significant visual changes at evaluation time, including alterations to the background, modifications to table texture and robot appearance, and the addition of irrelevant objects to the scene. An example of these perturbations for the box-v1 task is shown in Figure 1.

We compare three variants: the *Vanilla Diffusion Policy*, trained and evaluated on unmodified RGB images; the *Masked Diffusion Policy*, which segments the task-relevant objects—specifically the gripper and manipulated object—and places them on a plain black background by masking out all other regions; and *ARRO*, which uses the same segmentation but overlays the task-relevant components onto a structured virtual grid background, providing a consistent and informative visual context. Figure 3 illustrates these representations for the box-v1 task. For each task and each model, we train the policy for 1000 epochs and evaluate on 10 trials.

As shown in Figure 3, ARRO consistently outperforms both baselines. The Vanilla Diffusion Policy suffers from substantial performance degradation across all scenarios due to its reliance on raw visual features, which no longer remain reliable under domain shifts. The Masked Diffusion Policy partially retains performance by removing distractors. However, it still performs noticeably worse than ARRO. This suggests that while masking suppresses irrelevant information, it may also discard useful visual cues that contribute to task execution. In contrast, ARRO not only filters out distractors but also reintroduces a structured and consistent background, improving robustness and the ability to generalize across varied visual conditions.

To complement the quantitative results, Figure 4 presents representative execution sequences using ARRO for the box-v1 and doll-v1 tasks. Notably, the segmentation module maintains reliable performance even under challenging conditions, such as partial occlusion (e.g., when the doll is partially blocked by the plush toy) or shape deformation (e.g., when the plush toy is grasped or the box begins to close). Despite the presence of visually complex and colorful objects—such as the multi-textured doll—the segmentation remains accurate throughout execution.

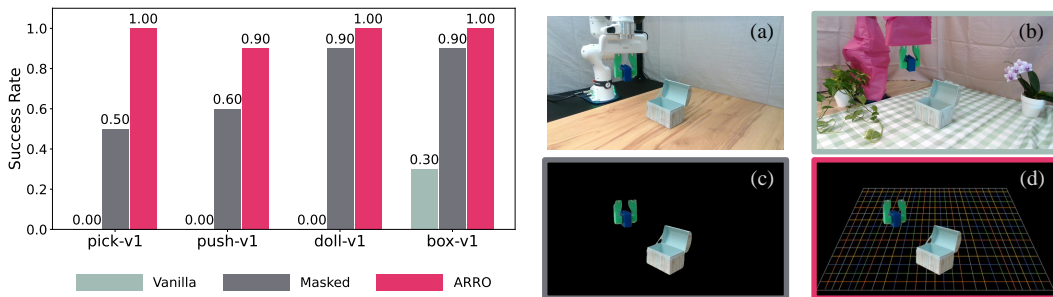


Figure 3: Performance comparison across four manipulation tasks (left) and visualization of input formats (right). (a) shows the training scene, while (b) depicts an altered scene with visual domain shifts used during inference. (c) and (d) illustrate the corresponding inputs for the masked diffusion policy and ARRO, respectively.

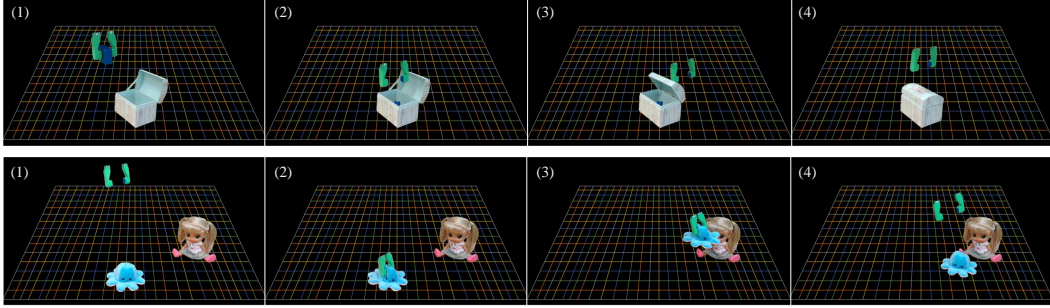


Figure 4: Execution sequences using ARRO on the Doll and Box tasks. By overlaying task-relevant segmentation regions on a virtual background, ARRO neutralizes the effect of visual domain shifts.

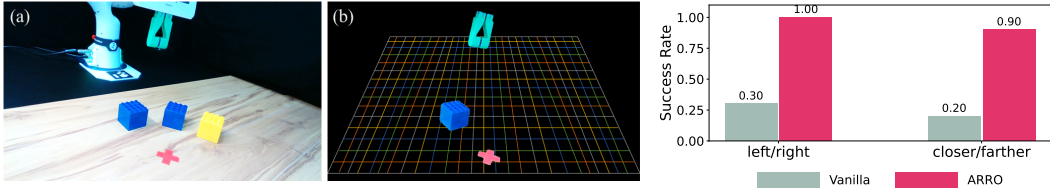


Figure 5: Handling distractor objects. *Left*: example input image with distractors (a) and the ARRO-segmented version (b) where the task is to “Push the *blue cube that is farther from the yellow cube* to the red cross”. *Right*: success rates for the spatial reasoning tasks.

4.1.2 Handling Distractor Objects

To assess whether ARRO can handle distractor objects and enable spatial reasoning, we repeat the push experiment with additional distractor items in the scene. Specifically, we investigate whether the vision-language model can move beyond basic object recognition (e.g., selecting “the blue cube”) to spatial grounding, such as identifying *the blue cube farther from the yellow cube*.

We design two spatial reasoning tasks to evaluate whether the system can correctly identify and act upon objects based on spatial relationships. In the first task, the robot must “push the *blue cube on the left/right* to the red cross.” In the second, it must “push the *blue cube that is closer to/farther from the yellow cube* to the red cross.” Once the vision-language model identifies the correct task-relevant object, ARRO masks out all other image regions—including distractor objects—ensuring that the policy operates solely on the relevant visual input.

In both tasks, ARRO demonstrates strong performance and reliably selects the appropriate object based on the spatial relation described in the instruction. In contrast, the vanilla diffusion policy exhibits a substantial drop in performance. It frequently fails to identify the correct object, sometimes selecting a distractor, switching targets mid-execution, or moving ambiguously between multiple candidates. Even when the correct object is selected, the resulting motion is often imprecise. These results highlight ARRO’s robustness to distractors and its capacity to support spatially grounded reasoning in visually complex environments.

4.1.3 Generalist Policies

In this section, we investigate whether ARRO can also benefit generalist policies. We evaluate two language-conditioned generalist models—Octo [15] and OpenVLA [16]—on the pick and push tasks, using the pick-v1 and push-v1 datasets for training, respectively. The results are presented in Table 1. For clearer comparison, we also report the success rates of the vanilla variants evaluated under the same visual domain as used during training. As shown in the table, both the Masked and ARRO variants consistently outperform their vanilla counterparts in settings where the visual domain is altered at evaluation time. In some cases, the degradation in performance of the vanilla

Table 1: Success rates of OpenVLA and Octo on the push and pick tasks under modified visual conditions. Each model is trained on the original scene and evaluated either under the same or visually altered scene.

Policy	Push			Pick			
	Same scene Vanilla	Altered scene Vanilla	Altered scene ARRO	Same scene Vanilla	Altered scene Vanilla	Altered scene Masked	Altered scene ARRO
Octo	0.3	0	0.10	0.5	0	0.3	0.4
OpenVLA	0.1	0	0.05	0.6	0	0.4	0.4

variant under domain shifts results in abrupt and unpredictable behavior, raising safety concerns for real-world deployment.

4.2 ARRO in Simulation

In addition to the real-world experiments, we also evaluate ARRO in simulation on the tasks pick-v2 and sim-pick-v2. Unlike in pick-v1 the cube is red and we collected the demonstrations automatically both in the real world and in simulation. We investigate whether ARRO can help mitigate the sim-to-real gap [18] and facilitate cross-embodiment policy transfer. Figure 6 illustrates our experimental setup: the physical setup in our lab using the FR3 robot, its replication in a MuJoCo [49] simulation environment, and a cross-embodiment variant where the FR3 is replaced by a UR5e robotic arm within the same simulated setting.

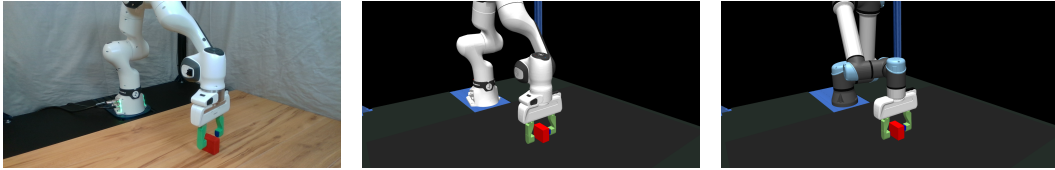


Figure 6: Experimental setup for the picking task in two environments and one cross-embodiment scenario *Left to right*: Real-world FR3 setup, model of the setup in MuJoCo used for collecting sim-pick-v2, and UR5e setup for cross-embodiment experiments in MuJoCo.

4.2.1 Real-to-Sim

To test the real-to-sim performance, we trained Diffusion Policy, Octo, and OpenVLA on the pick-v2 dataset and evaluated the task success rates for two settings: The unmodified real-world scene and the replicated scene in the simulation. We trained Octo and Open VLA on pick-v2 and Diffusion Policy, as indicated by the asterisk, on pick-v1. We evaluated the trained policies in-distribution on the same unchanged setup on 10 episodes (real-to-real success rate) and out-of-distribution on a replicated MuJoCo setup on 100 episodes (real-to-sim success rate). As shown in Table 2, all models have decent real-world performance, but drop to 0% success rate when evaluated in simulation. However, when using ARRO and black masking, OpenVLA is able to retain about half of its real-world performance. Octo still drops to almost 0% but at least shows some form of learned behavior. Diffusion Policy does not exhibit any immediate transfer in terms of success rate, which can be attributed, at least in part, to the smaller training dataset and differences in the vision backbone architecture. In addition to the success rates in the real-to-sim experiments, we computed reward values using a simple distance metric inspired by ManiSkill [50]. The results are shown in Figure 7. Both ARRO and the simple masked background yield higher rewards than the vanilla baselines.

4.2.2 Cross-Embodiment

To test the cross-embodiment capabilities of ARRO, we train our policies on a simulation dataset, referred to as sim-pick-v2, using the FR3 and test it on a UR5e embodiment. We evaluate both in-distribution on the training environment for 100 episodes (sim-to-sim success rate) and on the new

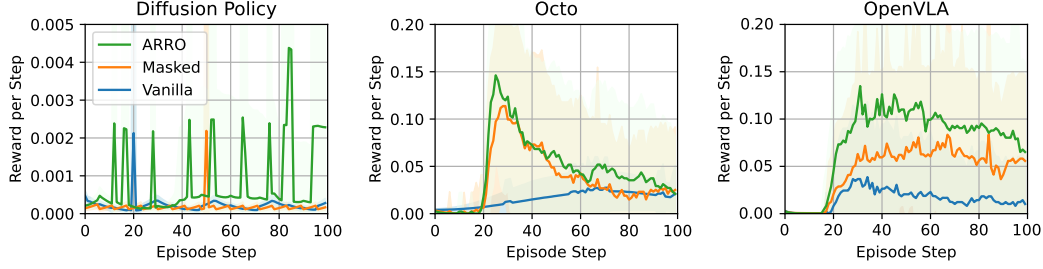


Figure 7: Normalized mean evaluation reward per step averaged over 100 episodes on the pick cube task in simulation on the FR3 (same embodiment). All models were trained on the pick-v1 real-world dataset. Shaded areas indicate standard deviations.

UR5e embodiment for 100 episodes (cross-embodiment success rate). The results are presented in Table 2. The diffusion policy’s performance drops to 0 when evaluated on a novel embodiment, which is expected given that it was trained exclusively on the FR3 robot. In contrast, both the masking approach and ARRO exhibit only a minor reduction in success rates. This is likely because the embodiment change has minimal impact on the diffusion policy: the visual input remains largely unaffected due to the masking of the robot body, and the control commands are issued in absolute Cartesian space, which remains invariant to the embodiment.

Octo and OpenVLA also exhibit reduced drops in success rates when combined with ARRO and masking. Unlike the diffusion policy, their performance does not fall to zero, and they retain a degree of success on the new embodiment. This can be attributed to their larger and more diverse training datasets, which are explicitly designed to support cross-embodiment generalization. As a result, both models encountered the UR5 robot during training, facilitating better transfer even in simulation settings.

Table 2: Real-to-sim and cross-embodiment success performance of vanilla (V), masked (M) and ARRO (ours) versions of different policies. See sections 4.2.1 and 4.2.2 for details.

Policy	real-to-real			real-to-sim			sim-to-sim			cross-embodiment		
	V	M	ours	V	M	ours	V	M	ours	V	M	ours
Diffusion	1.0*	0.5*	1.0*	0	0.00	0.00	0.95	0.15	1.00	0.00	0.12	0.99
Octo	0.5	0.3	0.4	0	0.01	0.02	0.17	0.08	0.16	0.12	0.07	0.14
OpenVLA	0.6	0.4	0.4	0	0.16	0.22	0.14	0.50	0.51	0.04	0.36	0.41

5 Conclusion

In this paper, we presented ARRO, a calibration-free visual augmentation pipeline that improves the robustness of visuomotor policies. By segmenting and retaining only task-relevant regions and overlaying them on a structured virtual background, ARRO enhances generalization without retraining or camera calibration. Our experiments in both real-world and simulated settings demonstrate consistent performance gains for task-specific as well as generalist policies. ARRO thus offers a lightweight and scalable solution for robust robotic manipulation in visually diverse environments.

Looking ahead, an interesting line of research is to apply ARRO at scale using data from the Open X-Embodiment dataset collection [12] to explore its potential for enhancing cross-task and cross-embodiment generalization. Another promising direction is the integration of ARRO with reinforcement learning pipelines to assess its benefits in online policy adaptation. Taken together, these future directions may further expand the applicability of ARRO toward more general, robust, and scalable robotic learning systems.

6 Limitations

Segmentation Models ARRO builds on recent advances in vision foundation models for zero-shot image segmentation. Therefore, our approach’s performance depends strongly on the performance of the underlying models, both with respect to the quality of the segmentation and inference time. While our experiments required basic prompt engineering to robustly identify the desired points provided to the segmentation model, no other fine-tuning was needed. We are aware that this may be different for other setups and environments. In particular, the additional latency introduced by the segmentation can be challenging for time-critical tasks with real-time constraints. But while we use SAM 2 [47] and GroundingDINO [46] to generate segmentation masks and select objects, our pipeline is not specific to these models. Replacing them with alternatives that have desirable properties for a particular task, robot, or environment can be expected to directly enhance the performance of ARRO. For example, replacing SAM 2 by a basic task-optimized segmentation algorithm will reduce both latency and resource requirements.

Dynamic Scenes The approach to segmentation currently implemented by ARRO assumes that all task-relevant objects are known and visible at the beginning of an episode for initialization. These assumptions are not met if objects enter the scene dynamically or change during an episode, e.g., during a disassembly task. In this case, the prompts for the segmentation model need to be updated dynamically, which requires additional tracking of the task. This can be accomplished by querying the vision-language model that is also used for initialization after relevant robot actions to analyze the scene and adapt the segmentation prompt as required.

Robot Gripper In our experiments, we use gripper fingers with a clearly visible color, which makes it easy to detect and segment them. This is in line with previous work on visuomotor learning [25]. Segmenting other gripper designs can be more challenging. This can be addressed by moving the robot to a pre-defined home position at the beginning of an episode and initializing the segmentation model with a fixed set of bounding boxes. If camera calibration data is available, the boxes can be generated automatically.

Lighting and Reflections ARRO generates an environment-independent scene representation by removing distractors and applying a standardized background. However, it does not handle changes of the scene that affect the visual appearance of task-related objects, such as lighting and reflections. While lighting was shown to have a modest impact on task performance, strong reflections may appear like changed textures and change the visual appearance significantly [17]. A possible solution that would not only address this issue but also add robustness against other changes of an object’s appearance is to apply image inpainting, which was successfully used in earlier work [39].

Acknowledgments

The authors gratefully acknowledge the scientific support and HPC resources provided by the Erlangen National High Performance Computing Center (NHR@FAU) of the Friedrich-Alexander-Universität Erlangen-Nürnberg (FAU) under the BayernKI project no. v108be. BayernKI funding is provided by Bavarian state authorities.

References

- [1] A. Vaswani, N. Shazeer, N. Parmar, J. Uszkoreit, L. Jones, A. N. Gomez, Ł. ukasz Kaiser, and I. Polosukhin. Attention is All you Need. In *Advances in Neural Information Processing Systems*, volume 30. Curran Associates, Inc., 2017.
- [2] J. Ho, A. Jain, and P. Abbeel. Denoising Diffusion Probabilistic Models. In *Advances in Neural Information Processing Systems*, volume 33, pages 6840–6851. Curran Associates, Inc., 2020.
- [3] A. Dosovitskiy, L. Beyer, A. Kolesnikov, D. Weissenborn, X. Zhai, T. Unterthiner, M. Dehghani, M. Minderer, G. Heigold, S. Gelly, J. Uszkoreit, and N. Houlsby. An Image is Worth 16x16 Words: Transformers for Image Recognition at Scale, June 2021.
- [4] C. Chi, Z. Xu, S. Feng, E. Cousineau, Y. Du, B. Burchfiel, R. Tedrake, and S. Song. Diffusion policy: Visuomotor policy learning via action diffusion. *Int. Journal of Robotics Research (IJRR)*, page 02783649241273668, 2023.
- [5] Y. Zhu, A. Joshi, P. Stone, and Y. Zhu. Viola: Imitation learning for vision-based manipulation with object proposal priors. In *Proc. of the Conf. on Robot Learning (CoRL)*, pages 1199–1210, 2023.
- [6] M. Dalal, A. Mandlekar, C. Garrett, A. Handa, R. Salakhutdinov, and D. Fox. Imitating task and motion planning with visuomotor transformers. *arXiv preprint arXiv:2305.16309*, 2023.
- [7] H. R. Walke, K. Black, T. Z. Zhao, Q. Vuong, C. Zheng, P. Hansen-Estruch, A. W. He, V. Myers, M. J. Kim, M. Du, A. Lee, K. Fang, C. Finn, and S. Levine. BridgeData V2: A Dataset for Robot Learning at Scale. In *Proc. of the Conf. on Robot Learning (CoRL)*, pages 1723–1736. PMLR, 2023.
- [8] Z. Fu, T. Z. Zhao, and C. Finn. Mobile ALOHA: Learning Bimanual Mobile Manipulation with Low-Cost Whole-Body Teleoperation, Jan. 2024.
- [9] H. Bharadhwaj, J. Vakil, M. Sharma, A. Gupta, S. Tulsiani, and V. Kumar. RoboAgent: Generalization and Efficiency in Robot Manipulation via Semantic Augmentations and Action Chunking. In *Proc. of the IEEE Int. Conf. on Robotics & Automation (ICRA)*, pages 4788–4795, 2024.
- [10] H.-S. Fang, H. Fang, Z. Tang, J. Liu, C. Wang, J. Wang, H. Zhu, and C. Lu. RH20T: A Comprehensive Robotic Dataset for Learning Diverse Skills in One-Shot. In *Proc. of the IEEE Int. Conf. on Robotics & Automation (ICRA)*, pages 653–660, May 2024.
- [11] A. Khazatsky, K. Pertsch, S. Nair, A. Balakrishna, S. Dasari, S. Karamcheti, S. Nasiriany, M. K. Srirama, L. Y. Chen, K. Ellis, P. D. Fagan, J. Hejna, M. Itkina, M. Lepert, Y. J. Ma, P. T. Miller, J. Wu, S. Belkhale, S. Dass, H. Ha, A. Jain, A. Lee, Y. Lee, M. Memmel, S. Park, I. Radosavovic, K. Wang, A. Zhan, K. Black, C. Chi, K. B. Hatch, S. Lin, J. Lu, J. Mercat, A. Rehman, P. R. Sanketi, A. Sharma, C. Simpson, Q. Vuong, H. R. Walke, B. Wulfe, T. Xiao, J. H. Yang, A. Yavary, T. Z. Zhao, C. Agia, R. Baijal, M. G. Castro, D. Chen, Q. Chen, T. Chung, J. Drake, E. P. Foster, J. Gao, V. Guizilini, D. A. Herrera, M. Heo, K. Hsu, J. Hu, M. Z. Irshad, D. Jackson, C. Le, Y. Li, K. Lin, R. Lin, Z. Ma, A. Maddukuri, S. Mirchandani, D. Morton, T. Nguyen, A. O’Neill, R. Scalise, D. Seale, V. Son, S. Tian, E. Tran, A. E. Wang, Y. Wu, A. Xie, J. Yang, P. Yin, Y. Zhang, O. Bastani, G. Berseth, J. Bohg, K. Goldberg,

- A. Gupta, A. Gupta, D. Jayaraman, J. J. Lim, J. Malik, R. Martín-Martín, S. Ramamoorthy, D. Sadigh, S. Song, J. Wu, M. C. Yip, Y. Zhu, T. Kollar, S. Levine, and C. Finn. Droid: A large-scale in-the-wild robot manipulation dataset. *arXiv preprint arXiv:2403.12945*, 2025.
- [12] A. O’Neill, A. Rehman, A. Maddukuri, A. Gupta, A. Padalkar, A. Lee, A. Pooley, A. Gupta, A. Mandlekar, A. Jain, et al. Open x-embodiment: Robotic learning datasets and rt-x models: Open x-embodiment collaboration 0. In *Proc. of the IEEE Int. Conf. on Robotics & Automation (ICRA)*, pages 6892–6903, 2024.
- [13] A. Brohan, N. Brown, J. Carbajal, Y. Chebotar, J. Dabis, C. Finn, K. Gopalakrishnan, K. Hausman, A. Herzog, J. Hsu, et al. Rt-1: Robotics transformer for real-world control at scale. *arXiv preprint arXiv:2212.06817*, 2022.
- [14] A. Brohan, N. Brown, J. Carbajal, Y. Chebotar, X. Chen, K. Choromanski, T. Ding, D. Driess, A. Dubey, C. Finn, et al. Rt-2: Vision-language-action models transfer web knowledge to robotic control. *arXiv preprint arXiv:2307.15818*, 2023.
- [15] O. M. Team, D. Ghosh, H. Walke, K. Pertsch, K. Black, O. Mees, S. Dasari, J. Hejna, T. Kreiman, C. Xu, et al. Octo: An open-source generalist robot policy. *arXiv preprint arXiv:2405.12213*, 2024.
- [16] M. J. Kim, K. Pertsch, S. Karamcheti, T. Xiao, A. Balakrishna, S. Nair, R. Rafailov, E. Foster, G. Lam, P. Sanketi, et al. Openvla: An open-source vision-language-action model. *arXiv preprint arXiv:2406.09246*, 2024.
- [17] A. Xie, L. Lee, T. Xiao, and C. Finn. Decomposing the generalization gap in imitation learning for visual robotic manipulation. *arXiv preprint arXiv:2307.03659*, 2023.
- [18] X. Li, K. Hsu, J. Gu, K. Pertsch, O. Mees, H. R. Walke, C. Fu, I. Lunawat, I. Sieh, S. Kirmani, S. Levine, J. Wu, C. Finn, H. Su, Q. Vuong, and T. Xiao. Evaluating Real-World Robot Manipulation Policies in Simulation, May 2024.
- [19] J. Tobin, R. Fong, A. Ray, J. Schneider, W. Zaremba, and P. Abbeel. Domain randomization for transferring deep neural networks from simulation to the real world. In *Proc. of the IEEE/RSJ Int. Conf. on Intelligent Robots and Systems (IROS)*, 2017.
- [20] Y. Chebotar, A. Handa, V. Makoviychuk, M. Macklin, J. Issac, N. Ratliff, and D. Fox. Closing the sim-to-real loop: Adapting simulation randomization with real world experience. In *Proc. of the IEEE Int. Conf. on Robotics & Automation (ICRA)*, pages 8973–8979, 2019.
- [21] A. S. Chen, S. Nair, and C. Finn. Learning generalizable robotic reward functions from” in-the-wild” human videos. *arXiv preprint arXiv:2103.16817*, 2021.
- [22] H. Xiong, Q. Li, Y.-C. Chen, H. Bharadhwaj, S. Sinha, and A. Garg. Learning by watching: Physical imitation of manipulation skills from human videos. In *Proc. of the IEEE/RSJ Int. Conf. on Intelligent Robots and Systems (IROS)*, pages 7827–7834, 2021.
- [23] M. Lepert, J. Fang, and J. Bohg. Phantom: Training robots without robots using only human videos. *arXiv preprint arXiv:2503.00779*, 2025.
- [24] J. Yang, D. Sadigh, and C. Finn. Polybot: Training one policy across robots while embracing variability. *arXiv preprint arXiv:2307.03719*, 2023.
- [25] C. Chi, Z. Xu, C. Pan, E. Cousineau, B. Burchfiel, S. Feng, R. Tedrake, and S. Song. Universal manipulation interface: In-the-wild robot teaching without in-the-wild robots. *arXiv preprint arXiv:2402.10329*, 2024.
- [26] C. Devin, P. Abbeel, T. Darrell, and S. Levine. Deep Object-Centric Representations for Generalizable Robot Learning. In *Proc. of the IEEE Int. Conf. on Robotics & Automation (ICRA)*, 2018.

- [27] A. Zeng, P. Florence, J. Tompson, S. Welker, J. Chien, M. Attarian, T. Armstrong, I. Krasin, D. Duong, V. Sindhwani, and J. Lee. Transporter Networks: Rearranging the Visual World for Robotic Manipulation. In *Proc. of the Conf. on Robot Learning (CoRL)*, 2021.
- [28] M. Shridhar, L. Manuelli, and D. Fox. CLIPort: What and Where Pathways for Robotic Manipulation. In *Proc. of the Conf. on Robot Learning (CoRL)*, 2022.
- [29] M. Sieb, Z. Xian, A. Huang, O. Kroemer, and K. Fragkiadaki. Graph-Structured Visual Imitation. In *Proc. of the Conf. on Robot Learning (CoRL)*, 2020.
- [30] L. Manuelli, W. Gao, P. Florence, and R. Tedrake. KPAM: KeyPoint Affordances for Category-Level Robotic Manipulation. In T. Asfour, E. Yoshida, J. Park, H. Christensen, and O. Khatib, editors, *Robotics Research*, 2022.
- [31] W. Huang, C. Wang, Y. Li, R. Zhang, and L. Fei-Fei. ReKep: Spatio-Temporal Reasoning of Relational Keypoint Constraints for Robotic Manipulation. In *Proc. of the Conf. on Robot Learning (CoRL)*, 2024.
- [32] S. Nasiriany, F. Xia, W. Yu, T. Xiao, J. Liang, I. Dasgupta, A. Xie, D. Driess, A. Wahid, Z. Xu, Q. Vuong, T. Zhang, T.-W. E. Lee, K.-H. Lee, P. Xu, S. Kirmani, Y. Zhu, A. Zeng, K. Hausman, N. Heess, C. Finn, S. Levine, and B. Ichter. PIVOT: Iterative Visual Prompting Elicits Actionable Knowledge for VLMs. In *Proceedings of the 41st International Conference on Machine Learning*, 2024.
- [33] K. Fang, F. Liu, P. Abbeel, and S. Levine. Moka: Open-world robotic manipulation through mark-based visual prompting. *Robotics: Science and Systems (RSS)*, 2024.
- [34] S. Nair, A. Rajeswaran, V. Kumar, C. Finn, and A. Gupta. R3M: A Universal Visual Representation for Robot Manipulation. In *Proc. of the Conf. on Robot Learning (CoRL)*, 2022.
- [35] S. Karamcheti, S. Nair, A. S. Chen, T. Kollar, C. Finn, D. Sadigh, and P. Liang. Language-Driven Representation Learning for Robotics. *arXiv preprint arXiv:2302.12766*, 2023.
- [36] S. Chen, R. Garcia, I. Laptev, and C. Schmid. SUGAR: Pre-training 3D Visual Representations for Robotics. In *Proc. of the Int. Conf. on Computer Vision (ICCV)*, 2024.
- [37] Z. Mandi, H. Bharadhwaj, V. Moens, S. Song, A. Rajeswaran, and V. Kumar. Cacti: A framework for scalable multi-task multi-scene visual imitation learning. *arXiv preprint arXiv:2212.05711*, 2022.
- [38] T. Yu, T. Xiao, A. Stone, J. Tompson, A. Brohan, S. Wang, J. Singh, C. Tan, J. Peralta, B. Ichter, et al. Scaling robot learning with semantically imagined experience. *arXiv preprint arXiv:2302.11550*, 2023.
- [39] Z. Chen, S. Kiami, A. Gupta, and V. Kumar. Genaug: Retargeting behaviors to unseen situations via generative augmentation. *arXiv preprint arXiv:2302.06671*, 2023.
- [40] H. Bharadhwaj, J. Vakil, M. Sharma, A. Gupta, S. Tulsiani, and V. Kumar. Roboagent: Generalization and efficiency in robot manipulation via semantic augmentations and action chunking. In *Proc. of the IEEE Int. Conf. on Robotics & Automation (ICRA)*, pages 4788–4795, 2024.
- [41] M. Shridhar, Y. L. Lo, and S. James. Generative image as action models. *arXiv preprint arXiv:2407.07875*, 2024.
- [42] J. Zhang, L. Tai, P. Yun, Y. Xiong, M. Liu, J. Boedecker, and W. Burgard. Vr-goggles for robots: Real-to-sim domain adaptation for visual control. *IEEE Robotics and Automation Letters*, 4(2):1148–1155, 2019.

- [43] L. Y. Chen, K. Hari, K. Dharmarajan, C. Xu, Q. Vuong, and K. Goldberg. Mirage: Cross-embodiment zero-shot policy transfer with cross-painting. *arXiv preprint arXiv:2402.19249*, 2024.
- [44] M. Lepert, R. Doshi, and J. Bohg. Shadow: Leveraging segmentation masks for cross-embodiment policy transfer. *arXiv preprint arXiv:2503.00774*, 2025.
- [45] L. Y. Chen, C. Xu, K. Dharmarajan, M. Z. Irshad, R. Cheng, K. Keutzer, M. Tomizuka, Q. Vuong, and K. Goldberg. Rovi-aug: Robot and viewpoint augmentation for cross-embodiment robot learning. *arXiv preprint arXiv:2409.03403*, 2024.
- [46] S. Liu, Z. Zeng, T. Ren, F. Li, H. Zhang, J. Yang, Q. Jiang, C. Li, J. Yang, H. Su, J. Zhu, and L. Zhang. Grounding dino: Marrying dino with grounded pre-training for open-set object detection. In A. Leonardis, E. Ricci, S. Roth, O. Russakovsky, T. Sattler, and G. Varol, editors, *Proc. of Europ. Conf. on Computer Vision (ECCV)*. Springer Nature Switzerland, 2025.
- [47] N. Ravi, V. Gabeur, Y.-T. Hu, R. Hu, C. Ryali, T. Ma, H. Khedr, R. Rädle, C. Rolland, L. Gustafson, et al. Sam 2: Segment anything in images and videos. *arXiv preprint arXiv:2408.00714*, 2024.
- [48] J. Achiam, S. Adler, S. Agarwal, L. Ahmad, I. Akkaya, F. L. Aleman, D. Almeida, J. Al-tenschmidt, S. Altman, and S. e. a. Anadkat. Gpt-4 technical report. <https://arxiv.org/abs/2303.08774>, 2023.
- [49] E. Todorov, T. Erez, and Y. Tassa. Mujoco: A physics engine for model-based control. In *Proc. of the IEEE/RSJ Int. Conf. on Intelligent Robots and Systems (IROS)*, 2012.
- [50] J. Gu, F. Xiang, X. Li, Z. Ling, X. Liu, T. Mu, Y. Tang, S. Tao, X. Wei, Y. Yao, X. Yuan, P. Xie, Z. Huang, R. Chen, and H. Su. ManiSkill2: A unified benchmark for generalizable manipulation skills. In *Proc. of the Int. Conf. on Learning Representations (ICLR)*, 2023.
- [51] K. Zakka, Y. Tassa, and MuJoCo Menagerie Contributors. MuJoCo Menagerie: A collection of high-quality simulation models for MuJoCo, 2022. URL http://github.com/google-deepmind/mujoco_menagerie.

A Appendix

A.1 ARRO Pseudocode

The pseudocode in Algorithm 1 and Algorithm 2 outlines the step-by-step process of the ARRO pipeline. It illustrates how our method segments the object and the gripper, tracks them across frames, and overlays them onto a virtual background to produce visually robust observations. We apply this procedure consistently during both training and inference to improve generalization under domain shifts.

Algorithm 1 ARRO Initialization

Input: I An RGB frame
 p_1^o, \dots, p_n^o Object prompts
 p^t A task prompt
Detect Open-vocabulary object detector (e.g., GroundingDINO)
Segment Uninitialized segmentation model (e.g., SAM2)
VLM Vision-language model (e.g., GPT-4o)

Output: The initialized segmentation model Segment_0

```

// Get object bounding boxes for complex objects
for  $p_i^o$  in  $\{p_1^o, \dots, p_n^o\}$  do
     $B_i = \text{Detect}(I, p_i^o)$ 
end for

// Get region masks to segment simple objects and gripper fingers
Run unprompted segmentation on  $I$  to get region masks:  $K_i \leftarrow \text{Segment}(I)$ 
Annotate keypoints in  $I$  with numeric labels to retrieve  $I^*$ 
Identify task-relevant keypoints in  $I^*$ :  $\{K_0, \dots, K_m\} \leftarrow \text{VLM}(I^*, p^t)$ 

// Initialize and return the segmentation model
return  $\text{Initialize}(\text{Segment}, I, B_0, \dots, B_n, K_0, \dots, K_m)$ 

```

Algorithm 2 ARRO Masking

Input: I RGB frame
 I_B RGB background image
 Segment_t Initialized segmentation model (e.g., SAM2)

Output: A masked RGB frame \tilde{I} and the updated segmentation model Segment_{t+1}

```

Track object and gripper masks:  $S^{\text{obj}}, S^{\text{gripper}}, \text{Segment}_{t+1}(I) \leftarrow \text{Segment}_t(I)$ 
Combine masks:  $S = S^{\text{obj}} \cup S^{\text{gripper}}$ 
Overlay  $S$  on virtual background  $I_B$  to recompose the scene into  $\tilde{I}$ 

return  $\tilde{I}, \text{Segment}_{t+1}$ 

```

A.2 Segmentation Initialization

As part of ARRO’s initialization process, we perform segmentation on the first frame of each episode to identify task-relevant components, including the robot gripper and target objects. To illustrate this process, Figure 8 shows the first frame of an episode after initial segmentation. Each region in the image is labeled with a numeric identifier. The annotated image is then provided to a vision-language model, such as GPT-4o, which is prompted to identify specific regions of interest—for instance, the *green gripper fingers*, the *red cross*, or the *blue cube that is farther from the yellow cube*. The model’s responses are visualized in the figure and demonstrate that it successfully identifies the correct regions.

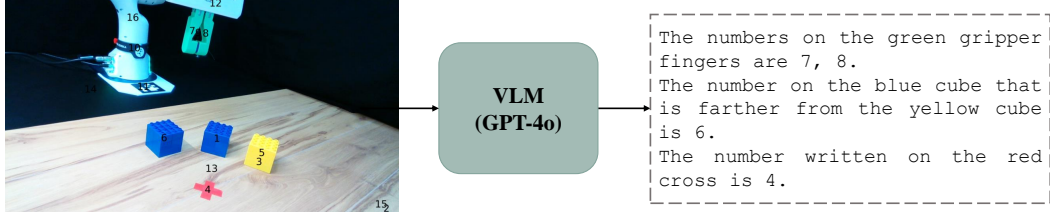


Figure 8: Illustration of segmentation initialization using a vision-language model (VLM). The input frame is segmented into regions and annotated with numeric labels, which have been enlarged for clarity. The annotated image is passed to GPT-4o, which identifies task-relevant elements such as the gripper fingers, the red cross, and the blue cube that is farther from the yellow cube. The model’s output demonstrates accurate recognition and spatial reasoning.

It is interesting to see that the VLM, beyond basic recognition, demonstrates spatial reasoning capabilities. In this example, it correctly selects the blue cube that is farther from the yellow one, despite the presence of multiple similar objects in the scene. This ability to reason about spatial relationships plays a crucial role in ensuring that ARRO consistently extracts only task-relevant visual information under diverse and potentially ambiguous scene configurations.

A.3 Handling Oclusions in ARRO

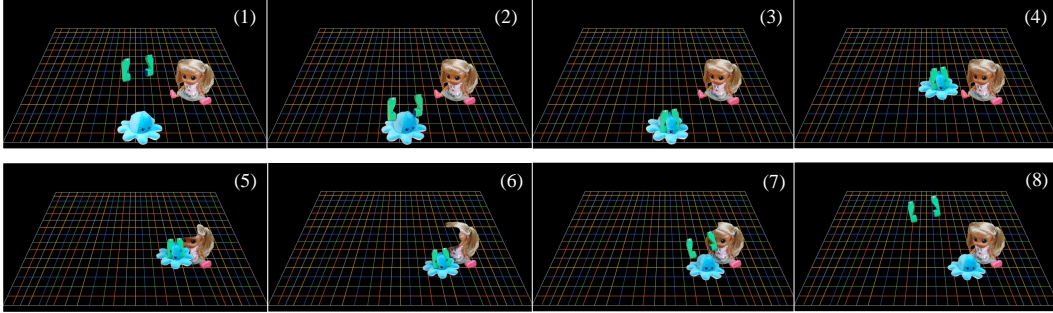


Figure 9: ARRO’s segmentation remains robust to transient occlusions caused by the robot arm or other objects. The doll is temporarily occluded in frames (5)–(7), but its segmentation accurately reappears once the occlusion clears, without manual correction.

Partial occlusions of objects may arise during certain tasks, either due to the robot’s own movements or the presence of other objects within the scene, as illustrated in Figure 9. In frames (5), (6), and (7), the doll is partially obscured—either by the robot arm or by the octopus plush toy temporarily blocking the view. Despite these transient occlusions, ARRO’s segmentation remains stable and accurate. As shown in the figure, once the occlusion subsides, the segmentation of the doll reliably reappears without requiring manual intervention or additional adjustment. This demonstrates that our segmentation pipeline is robust to temporary occlusions and consistently preserves the identification of task-relevant objects over time.

A.4 Datasets

We collected the datasets using both manual robot teleoperation and motion planning on a Franka Research 3 (FR3) robot arm. Each step of an episode contains the complete robot state, including joint positions and end effector pose, as well as a third-person view camera image of the scene with an RGB resolution of 1280×720 .

Real-World Teloperation The datasets pick-v1, push-v1, box-v1, and doll-v1 were collected manually through teleoperation. As some of the tasks were collected for other experiments, the

number of episodes varied across datasets, ranging from about 90 to about 260. In a preprocessing step, episodes were trimmed to remove time steps with zero actions.

Real-World and Simulation Motion Planning pick-v2 and sim-pick-v2 were collected automatically using a motion planner implemented by us. The pick-v2 dataset contains 463 episodes of the Franka Research 3 (FR3) picking up a red cube on our real-world lab setup. An episode contains 40 steps. The sim-pick-v2 dataset is a replication of the pick-v2 in a MuJoCo [49] simulation. We recorded it with the same motion planner, and, thus, it also has 40 steps per episode. The sim-pick-v2 dataset contains 900 episodes.

Segmentation We generated two segmented variants for each dataset, one with a black background and one with the background pattern described in the paper. For training, the datasets were converted to the data formats required by the different models.

A.5 Training

We trained checkpoints Diffusion Policy (DP) [4], Octo [15], and OpenVLA [16] using the code and parameters published with these policies.

Diffusion Policy We trained policies for pick-v1, push-v1, box-v1, doll-v1, pick-v2, and sim-pick-v2 with a ResNet-18 trained on ImageNet as observation encoder. We scaled the input images to 320x180 and applied a 90% random crop. The batch size was set to 16, and we trained the policies for up to 1000 epochs. For pick-v1, push-v1, box-v1, and doll-v1, a subset of 90 episodes was sampled for training, which corresponds to the size of the smallest of the four datasets. As pick-v2 and sim-pick-v2 were generated automatically and contain considerably more episodes, we trained on all episodes for 500 and 200 epochs, respectively.

Octo We fine-tuned the bigger octo-base-1.5 checkpoint for 20000 training steps on both the pick-v2 dataset and the sim-pick-v2 dataset. The batch size was set to 128 and the window size to one. We did a full fine-tuning which includes all weights of the model. Before training we resized the image to a resolution of 256×256 with a Lanczos filter. We used the following task instruction: “pick up the red cube”.

OpenVLA We fine-tuned OpenVLA for 20000 training steps on pick-v2 and sim-pick-v2 using the same task description as for Octo. We set the batch size to 6, used a learning rate of 2×10^{-5} and used no image augmentation. We did not use LoRA fine-tuning but instead fine-tuned the model fully. We also resized the images to a resolution of 256×256 with a Lanczos filter. OpenVLA internally resizes the image again to a resolution of 224×224 with a Letterbox filter. We used the same task instruction as for Octo.

A.6 Evaluation

We conducted all real-world experiments using a Franka Research 3 (FR3) robotic arm equipped with custom 3D-printed gripper fingers. Visual input was provided by an RGB camera in a third-person configuration and the policies executed actions in a closed-loop manner, conditioned on the incoming visual observations at each timestep. The action space used by the Diffusion Policy consisted of the absolute pose of the robot’s end-effector, parameterized by its Cartesian position (x, y, z) and orientation in roll-pitch-yaw angles (r, p, y) . An additional binary scalar was used to represent the gripper state, indicating whether the gripper should be open or closed. During inference, the action horizon of the Diffusion Policy was configured according to the temporal demands of each task, with a horizon of 14 steps for pick-v1 and box-v1, and 6 steps for push-v1 and doll-v1. The observation horizon consisted of two frames: the current RGB image and action at timestep t , along with those from the preceding timestep $t - 1$.

For each of the four manipulation tasks, we conducted ten evaluation trials per method: Vanilla, Masked, and ARRO. To ensure a fair and consistent comparison, we initialized each trial within the same set of predefined configurations, including the initial pose of the gripper and the position of the target object. This setup allowed us to control for variation in task conditions and isolate the impact of visual domain shifts on policy performance.

To evaluate robustness under domain shifts, we introduced a range of visual modifications at test time. These included changes to the background, table texture, and robot appearance, as well as the addition of distractor objects in the scene. Notably, in most cases, even minor alterations in the visual appearance of the environment led to significant degradation in the performance of the vanilla Diffusion Policy. In contrast, ARRO consistently maintained high success rates, demonstrating its ability to filter out task-irrelevant visual information and improve generalization across varied visual conditions. Our implementation details for diffusion policy are summarized in Table 3.

Table 3: Evaluation parameters for real-world tasks using Diffusion Policy.

Task	Action Horizon	Observation Horizon	Evaluation Trials
pick-v1	14	2	10
push-v1	6	2	10
box-v1	14	2	10
doll-v1	6	2	10

For our real-to-sim and our cross-embodiment experiments, we evaluated all three models for 100 episodes on our replicated MuJoCo setup. For the cross-embodiment experiment, we replaced the FR3 with a UR5e robot. All our robot models were taken from MuJoCo Menagerie [51].